

Physical properties of high-pressure synthesized $Al_{65}Cu_{20}Fe_{15}$ quasicrystal

Yibo Liu(刘一博), Changzeng Fan(范长增), Zhefeng Xu(许哲峰), Ruidong Fu(付瑞东), Feng Ke(柯峰), Lin Wang(王霖), Bin Wen(温斌), Lifeng Zhang(张立峰), Marek Mihalkovič, and Bo Xu(徐波)

Citatio: Chin. Phys. B, 2025, 34 (**9**): 096103. DOI: 10.1088/1674-1056/add4fb
http://cpb.iphy.ac.cn; http://iopscience.iop.org/cpb

What follows is a list of articles you may be interested in

Heterogeneous TiC-based composite ceramics with high toughness

Xiaoci Ma(马孝慈), Yufei Ge(葛雨非), Yutong Hou(侯语同), Keyu Shi(施柯羽), Jiaqi Zhang(张佳琪), Gaoping Yue(岳高平), Qiang Tao(陶强), and Pinwen Zhu(朱品文)

Chin. Phys. B, 2025, 34 (**8**): 086104. DOI: 10.1088/1674-1056/add5c8

Pressure-induced superconductivity and phase transition in PbSe and PbTe

Yuyang Jiang(江宇阳), Cuiying Pei(裴翠颖), Qi Wang(王琦), Juefei Wu(吴珏霏), Lili Zhang(张丽丽), Chao Xiong(熊超), and Yanpeng Qi(齐彦鹏)

Chin. Phys. B, 2024, 33 (**12**): 126105. DOI: 10.1088/1674-1056/ad8ecc

Linear magnetoresistance and structural distortion in layered $SrCu_{4-x}P_2$ single crystals

Yong Nie(聂勇), Zheng Chen(陈正), Wensen Wei(韦文森), Huijie Li(李慧杰), Yong Zhang(张勇), Ming Mei(梅明), Yuanyuan Wang(王园园), Wenhai Song(宋文海), Dongsheng Song(宋东升), Zhaosheng Wang(王钊胜), Xiangde Zhu(朱相德), Wei Ning(宁伟), and Mingliang Tian(田明亮)

Chin. Phys. B, 2024, 33 (**1**): 016108. DOI: 10.1088/1674-1056/acf705

Application of silicon carbide temperature monitors in 49-2 swimming-pool test reactor

Guang-Sheng Ning(宁广胜), Li-Min Zhang(张利民), Wei-Hua Zhong(钟巍华), Sheng-Hong Wang(王绳鸿), Xin-Yu Liu(刘心语), Ding-Ping Wang(汪定平), An-Ping He(何安平), Jian Liu(刘健), and Chang-Yi Zhang(张长义)

Chin. Phys. B, 2023, 32 (**5**): 056102. DOI: 10.1088/1674-1056/acb41c

Structure, phase evolution and properties of Ta films deposited using hybrid high-power pulsed and DC magnetron co-sputtering

Min Huang(黄敏), Yan-Song Liu(刘艳松), Zhi-Bing He(何智兵), and Yong Yi(易勇)

Chin. Phys. B, 2022, 31 (**6**): 066101. DOI: 10.1088/1674-1056/ac43a9

Physical properties of high-pressure synthesized $Al_{65}Cu_{20}Fe_{15}$ quasicrystal

Yibo Liu(刘一博)[1], Changzeng Fan(范长增)[1,2,†], Zhefeng Xu(许哲峰)[1], Ruidong Fu(付瑞东)[1], Feng Ke(柯峰)[1], Lin Wang(王霖)[1], Bin Wen(温斌)[1], Lifeng Zhang(张立峰)[1,3], Marek Mihalkovič[4], and Bo Xu(徐波)[1]

[1] *State Key Laboratory of Metastable Materials Science and Technology, Yanshan University, Qinhuangdao* 066004, *China*
[2] *Hebei Key Laboratory for Optimizing Metal Product Technology and Performance, Yanshan University, Qinhuangdao* 066004, *China*
[3] *School of Mechanical and Materials Engineering, North China University of Technology, Beijing* 100144, *China*
[4] *Institute of Physics, Slovak Academy of Sciences*, 84511 *Bratislava, Slovakia*

(Received 27 February 2025; revised manuscript received 28 April 2025; accepted manuscript online 7 May 2025)

$Al_{65}Cu_{20}Fe_{15}$ bulk is synthesized with the high-pressure synthesis (HPS) method. Various analytical techniques, such as single crystal x-ray diffraction (SXRD), scanning electron microscopy equipped with energy-dispersive x-ray spectroscopy, and transmission electron microscopy, are employed to characterize the sintered bulk and confirmed its quasicrystalline structure. The electrical resistivity of the HPS quasicrystal specimen is measured from 2 K to 300 K, revealing a significantly elevated value in comparison to samples prepared via alternative methods. Nanoindentation testing demonstrates exceptional hardness and elastic modulus of our $Al_{65}Cu_{20}Fe_{15}$ quasicrystal, consistent with existing results. The ratio of hardness to elastic modulus further highlight the potential superior wear resistance of the $Al_{65}Cu_{20}Fe_{15}$ quasicrystal. Differential scanning calorimetry measurement conducted on the HPS $Al_{65}Cu_{20}Fe_{15}$ quasicrystals reveal a high melting point of 877 °C.

Keywords: $Al_{65}Cu_{20}Fe_{15}$ quasicrystal, resistivity, microhardness, high-pressure synthesis

PACS: 61.44.Br, 71.23.Ft

DOI: 10.1088/1674-1056/add4fb **CSTR:** 32038.14.CPB.add4fb

1. Introduction

Quasicrystals represent a unique class of materials that bridge the gap between crystalline and amorphous forms. Since the discovery by Shechtman *et al.* over four decades ago,[1] quasicrystals have remained a focus point in materials science and related disciplines due to their exceptional atomic arrangements and remarkable physical properties. Among these, Al–Cu–Fe quasicrystals have attracted significant attention as they are among the first stable icosahedral quasicrystals to be synthesized and the first naturally occurring quasicrystals to be identified.[2–4] Historically, the synthesis of quasicrystals has been explored through various methods, including strip casting, rapid solidification, and mechanical alloying, to investigate their nucleation and growth mechanisms.[2,5–15] Notably, Tsai *et al.* achieved the synthesis of millimeter-scale quasicrystals by melting AlCuFe alloy in an argon arc furnace followed by prolonged annealing.[2] Furthermore, AlCuFe quasicrystals have been extensively studied for their unique properties and potential applications, such as anticorrosion properties,[16–19] thermoelectric properties,[20–23] and mechanical stability and plasticity.[24–26]

Recent research has delved into the nucleation mechanism and phase composition of AlCuFe quasicrystals under high pressure,[27–29] replicating the extreme pressure and temperature conditions during the formation of these unique structures in meteorites.[30,31] These studies underscore the significant impact of pressure on metal properties such as melting and boiling points, density, thermal conductivity, and electrical conductivity.[32,33] High-pressure sintering (HPS), a novel material synthesis method, has been employed to investigate new phases and superconducting materials.[34,35] Furthermore, HPS has emerging as an effective method for synthesizing quasicrystals, with the advantage of reduced experimental duration. However, the thermal stability and physical properties of quasicrystalline samples synthesized via this method warrant further investigation.

In this study, $Al_{65}Cu_{20}Fe_{15}$ quasicrystalline material was successfully synthesized using HPS method. Our investigation primarily focused on elucidating its electrical properties, mechanical behavior, and thermal stability, thereby providing an empirical basis for the potential applications of quasicrystalline materials.

2. Experimental details

2.1. Synthesis

High-purity elemental powders of aluminum (Al, 99.5% purity), copper (Cu, 99.97% purity), and iron (Fe, 99.5% pu-

†Corresponding author. E-mail: chzfan@ysu.edu.cn

© 2025 Chinese Physical Society and IOP Publishing Ltd. All rights, including for text and data mining, AI training, and similar technologies, are reserved.

rity) were accurately weighed to a total mass of 5 grams in a stoichiometric ratio of 65:20:15, respectively. These powders were thoroughly mixed through grinding in an agate mortar for a duration exceeding 30 min to achieve a homogeneous mixture. The resultant uniformly mixed powders were then transferred into a 5 mm cemented carbide mold and compressed under a pressure ranging from 3 MPa to 4 MPa for 3 min, forming a cylindrical block with a diameter of 5 mm. This cylinder was subsequently placed into a pyrophyllite mold, as illustrated in Fig. 1, and subject to HPS using a six-anvil high pressure apparatus (CS-IB type). The synthesis process involved applying a pressure of 6 GPa, elevating the temperature to 1473 K for 30 min, then lowering the temperature to 1073 K for an additional 2-hour heating. After ceasing the heating, the pressure was gradually released, and the sample was carefully removed from the apparatus.

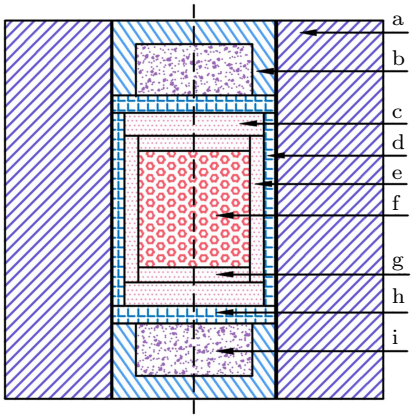


Fig. 1. Schematic diagram of high-pressure synthesis crucible assembly: a: pyrophyllite, b: conductive rims, c: boron nitride sheet, d: graphite furnace, e: boron nitride tube, f: sample, g: boron nitride sheet, h: graphite sheet, i: pyrophyllite and dolomite composite medium.

2.2. Characterizations

The structure of $Al_{65}Cu_{20}Fe_{15}$ alloy was analyzed using single crystal x-ray diffraction (SXRD, Bruker D8 Venture), employing Mo K_α radiation. Scanning electron microscopy (SEM) and energy-dispersive x-ray spectroscopy (EDX) tests were conducted on the HPS sample (supplementary materials). For the as-prepared HPS sample, two separate SEM/EDX tests have been conducted. In the first test, a Hitachi S4800 SEM equipped with EDX (EMAX, Japan) was utilized and a Hitachi S-3400N SEM equipped with EDX (EDAX Inc., USA) was utilized in the second test. The microstructure and crystalline state of synthesized $Al_{65}Cu_{20}Fe_{15}$ alloy were examined using transmission electron microscopy (TEM, FEI Talos F200X). TEM specimens were prepared by crushing a part of the HPS sample with agate mortar. The resultant powders were then combined with alcohol, transferred into a sample vial, and subjected to ultrasonic treatment for roughly 3 min. Using an eyedropper, 1–3 drops of the suspension were deposited onto a lacey support film. The sample was observed under TEM once it had dried.

Microhardness test was performed using a nanoindentation machine (Nano Indenter G200x), measuring 9 points on the sample surface with an indentation depth of 250 nm. The low-temperature resistivity (2 K–300 K) of the sample was measured using the Van der Pauw method in a home-built helium cryostat (CryoM-14T made from the Physike company). Thermal parameters were obtained using a differential scanning calorimeter (DSC, Netzsch STA449C) with a heating rate of 20 °C per minute.

3. Results and discussion

3.1. Structural characterization

The cylindrical product obtained from HPS, with a diameter of 5 mm, was initially sanded to remove the black contaminated surface layer and then thoroughly cleaned with anhydrous ethanol. A portion of the cylinder was subsequently cut off and crushed into powders. Using an optical microscope, a single particle with a flat surface and no visible flaws was selected, cleaned with anhydrous ethanol, and attached to the tip of a glass filament for XRD characterization. The Phi360 test, involving the rotation of the sample around the φ axis, was conducted on the selected particle (Fig. 2(a)). The diffraction patterns exhibited clear characteristic rings, indicating the polycrystallinity of the particle. The integral powder diffractions patterns were displayed in the right panel of Fig. 2(a). For comparison, Bragg's formula[36] was applied to convert the Bragg peaks from PDF card 00-042-1043[37] and XRD patterns from Tsai *et al.*,[38] both employing copper K_α radiation, to data corresponding to molybdenum radiation. As shown in Fig. 2(b), the main peaks of all three works align well, except that two small peaks do not present in the PDF card, as indicated by the dotted lines in Fig. 2(b). Given that the diffraction peaks from both the PDF card[37] and Tsai *et al.*[38] correspond to the $Al_{65}Cu_{20}Fe_{15}$ quasicrystalline phase, it can be concluded that the quasicrystalline $Al_{65}Cu_{20}Fe_{15}$ has been predominantly synthesized in this work with the HPS method. As illustrated in Fig. 2(b), the XRD peaks represented by the red line are broader. Scherer's formula was employed to qualitatively assess the grain size of the quasicrystals produced through the HPS method, as well as those reported by Tsai *et al*. The results indicated that the average grain size of the quasicrystals obtained via the HPS method was significantly smaller than that reported by Tsai *et al*., leading to a broad XRD peak. Subsequently, two independent SEM and EDX tests were carried out on the quasicrystalline samples obtained by high-pressure synthesis (see supplementary materials). The experimental results showed that the composition of the synthesized sample was in good agreement with the initial designed composition.

TEM observations were performed to further confirm the formation of quasicrystal phase. Figure 3(a) shows the bright

field TEM image of an Al–Cu–Fe specimen, which spans several microns laterally. Selected area electron diffraction (SAED) measurements were performed over the red-boxed region of the specimen, all the SAED patterns carrying out from the same region by rotating the specimen, revealing typical symmetrical features of quasicrystals, as illustrated in Figs. 3(b)–3(d). These diffraction spots correspond to the quasicrystal's two-fold, three-fold, and five-fold symmetrical orientations, respectively, clearly confirming the presence of quasicrystalline phases in the Al–Cu–Fe samples synthesized using the HPS method.

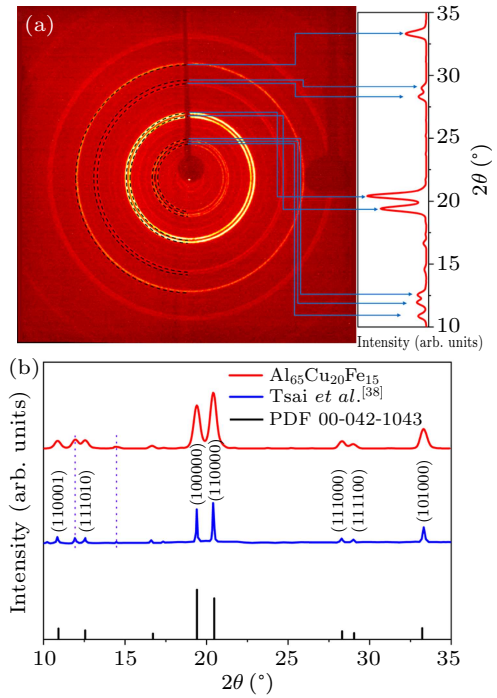


Fig. 2. XRD characterization of HPS-produced $Al_{65}Cu_{20}Fe_{15}$ alloy. (a) The Phi360 diffraction pattern of the high-pressure synthesis sample, (b) the powder diffraction pattern obtained by integrating the Phi360 diffraction pattern.

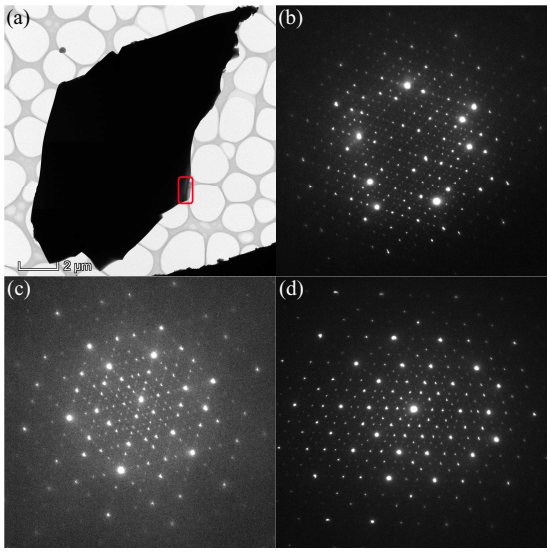


Fig. 3. Transmission electron micrographs taken from $Al_{65}Cu_{20}Fe_{15}$ quasicrystal of high-pressure synthesis: Diffraction pattern of (a) bright field image, (b) two-fold, (c) three-fold, (d) five-fold.

3.2. Electrical resistivity

Figure 4 shows the electrical resistivity of our quasicrystal $Al_{65}Cu_{20}Fe_{15}$ as a function of temperature. The resistivity increases from 5580 μΩ·cm at 300 K to 7280 μΩ·cm at 4.2 K. This behavior is characterized by a large negative temperature coefficient of resistivity (TCR), with a resistivity ratio ($\rho_{4.2\ K}/\rho_{300\ K}$) of approximately 1.3, which is consistent with values reported for other icosahedral AlCuFe quasicrystal.[39] In contrast, quasicrystals in the Al–Mn and Al–Cr systems exhibit an obvious positive TCR.[40,41] For comparison, a series of studies on the electrical resistivity of AlCuFe quasicrystals were reviewed,[42–44] and the resistivity of AlCuFe quasicrystals measured at 4.2 K are depicted in a bar chart in Fig. 4. The resistivity of $Al_{62}Cu_{25.5}Fe_{12.5}$ quasicrystals is the highest (9730 μΩ·cm) and that of $Al_{63}Cu_{25}Fe_{12}$ quasicrystals is the lowest (4300 μΩ·cm). Note that all these quasicrystals except ours were prepared using the melt spinning method. Interestingly, despite only slight compositional differences among the various quasicrystals depicted in Fig. 4, their resistivity values vary significantly, and our sample shows the second highest values among all listed samples. This discrepancy is likely attributable to the subtle structure variations in these quasicrystals. According to the research conducted by Klein *et al.* in 1990,[44] a higher purity of the quasicrystalline phase in the sample correlates with increased resistivity. This finding suggested that the synthesized sample possesses a highly pure quasicrystalline phase.

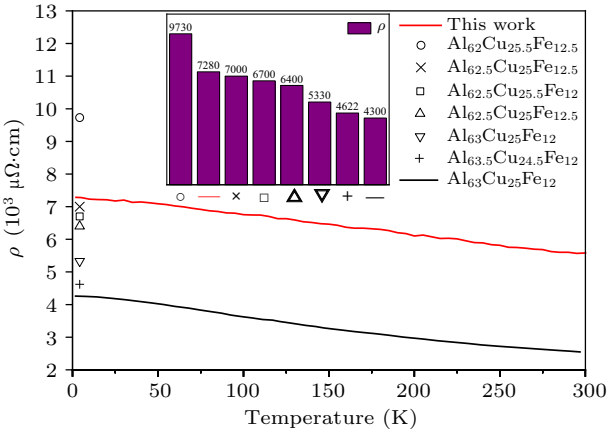


Fig. 4. The resistivity obtained from the experiment is compared with the literature.

3.3. Mechanical properties

The mechanical properties, specifically the Vickers hardness and elastic modulus of our $Al_{65}Cu_{20}Fe_{15}$ quasicrystalline alloy were measured using nanoindentation method. The indentation test was conducted on the sample surface using a 3×3 matrix, with a 30 μm interval between neighboring points to eliminate interference from adjacent tests. The indentation depth was set at about 250 nm. The individual values are then averaged to obtain the final results. As shown in Fig. 5, the measured Vickers hardness and elastic modulus are 12.4 GPa

and 199.5 GPa, respectively. The measured values are in good agreement with those reported in the literature,[45,46] demonstrating the reliability of our measurement. Quasicrystal materials are known for their excellent anti-friction properties, and the ratio of hardness to elastic modulus (H/E) is a reliable index for assessing the wear resistance of materials: The higher the H/E ratio, the greater the wear resistance.[47–49] In this study, the H/E of our $Al_{65}Cu_{20}Fe_{15}$ quasicrystalline alloy is 0.062. This value is more than double that of traditional aluminum alloys and maraging steel,[50,51] suggesting that the $Al_{65}Cu_{20}Fe_{15}$ quasicrystalline alloy is likely to exhibit favorable friction and wear properties.

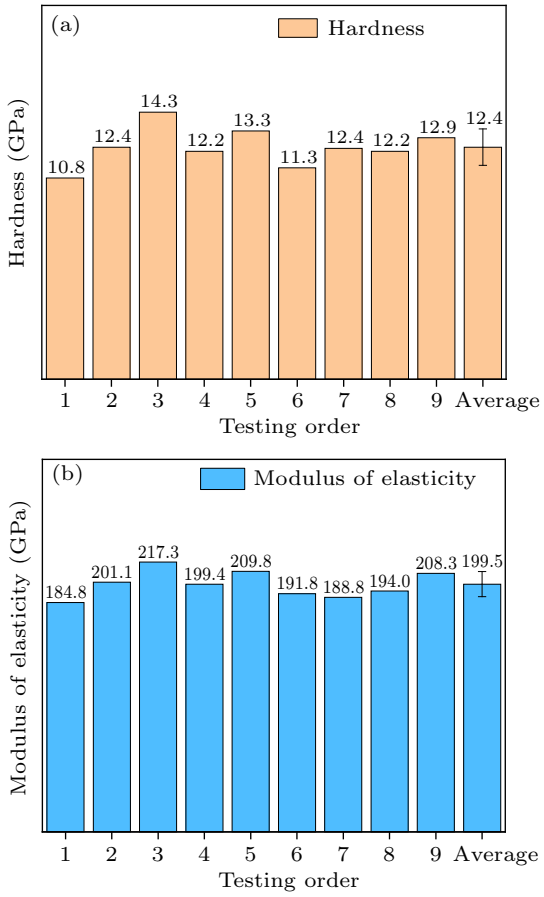


Fig. 5. Hardness (a) and elastic modulus (b) obtained from nanoindentation testing.

3.4. Thermal stability

Numerous studies have classified Al–Cu–Fe quasicrystals as thermodynamically stable.[2,52–54] However, the stability of Al–Cu–Fe quasicrystals produced using the HPS method need further confirmation. To investigate this, differential scanning calorimetry (DSC) tests was conducted from room temperature up to 900 °C. The results, as depicted in Fig. 6, show no phase change during heating up to the melting point (877 °C), suggesting thermodynamic stability of the quasicrystalline phase synthesized under high pressure. A significant observation is that the melting point of HPS quasicrystals is about 15 °C higher than that of the quasicrystals obtained from ambient pressure solidification,[2,52,55] underscoring a unique characteristic of our HPS sample. It is generally accepted that the melting point of substances will increase under high pressure.[56] As our quasicrystals sample were achieved by non-equilibrium rapid solidification at 6 GPa thus it should be different (with a higher melting point) from that obtained through equilibrium solidification under ambient pressure. The melting point of the $Al_{65}Cu_{20}Fe_{15}$ quasicrystal obtained via the non-equilibrium synthesis melt-spinning technique is 890 °C,[57] also much higher than that of Tsai *et al.*'s samples.[2] The detailed physical mechanism behind still needs to be clarified in future. Furthermore, the endothermic peak corresponding to the fusion occurs in a single stage, no splitting in the peak was observed, indicating that the $Al_{65}Cu_{20}Fe_{15}$ quasicrystal is predominantly composed of a single phase, which is quite similar to the earlier one reported for $Al_{65}Cu_{20}Fe_{15}$ by Tsai *et al.*[2] Additionally, the thermogravimetric (TG) curve measured during the DSC test, as shown in Fig. 6, indicates that the weight of the sample remained nearly constant throughout the heating process, further indicating the stability of the quasicrystalline phase.

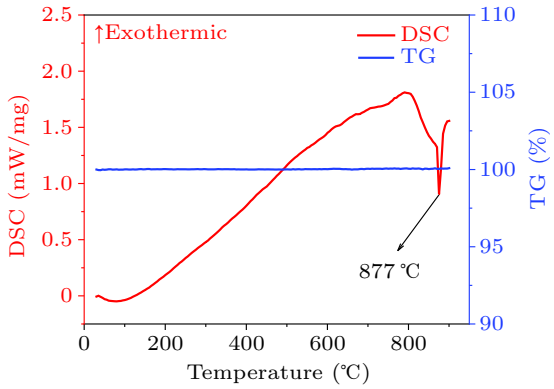


Fig. 6. DSC-TG test curve for samples synthesized by high-pressure synthesis.

4. Conclusion

To summarize, $Al_{65}Cu_{20}Fe_{15}$ quasicrystals were synthesized at high pressure and high temperature conditions and characterized with XRD, SEM/EDX, and TEM. Electrical resistivity measurement indicated that the present $Al_{65}Cu_{20}Fe_{15}$ quasicrystals exhibit high resistivity (the second highest observed) and a negative temperature coefficient of resistivity, implying that high pressure affects the formation and atomic arrangements of the quasicrystals. Nanoindentation tests showed that the hardness and elastic modulus values of our HPS $Al_{65}Cu_{20}Fe_{15}$ quasicrystals are comparable to those prepared by other methods. DSC measurement revealed that our quasicrystals start to melt at 795 °C and complete melting at 877 °C (melting point), which is 15 °C higher than that obtained through equilibrium solidification under ambient pressure. These findings are expected to stimulate further research into the formation and stability of quasicrystals.

Acknowledgements

Project supported by the National Natural Science Foundation of China (Grant Nos. 52173231 and 51925105), the Natural Science Foundation of Hebei Province, China (Grant No. E2022203182), and The Innovation Ability Promotion Project of Hebei supported by Hebei Key Laboratory for Optimizing Metal Product Technology and Performance (Grant No. 22567609H). Marek Mihalkovič has been supported by the grants from Slovak National Agencies (Grant Nos. VEGA 2/0144/21, APVV19-0369, and APVV-20-0124). Calculations were performed at the Computing Center of the Slovak Academy of Sciences using the supercomputing infrastructure acquired under Projects ITMS 26230120002 and 26210120002 and EuroHPC (Grant No. 101101903) (Supercomputer Devana).

References

[1] Shechtman D, Blech I, Gratias D and Cahn J W 1984 *Phys. Rev. Lett.* **53** 1951
[2] Tsai A P, Inoue A and Masumoto T 1987 *Jpn. J. Appl. Phys.* **26** L1505
[3] Bindi L, Steinhardt P J, Yao N and Lu P J 2009 *Science* **324** 1306
[4] Bindi L, Steinhardt P J, Yao N and Lu P J 2011 *Am. Mineral.* **96** 928
[5] Li C, Carey C, Li D, Caputo M, Bouch R and Hampikian H 2018 *Mater. Charact.* **140** 162
[6] Evangelista K and Cavalcante D 2021 *J. Mater. Res. Technol.* **15** 1496
[7] Aghaali V, Rahimipour M R, Faraji A and Ebadzadeh T 2024 *Mater. Today Commun.* **38** 107499
[8] Qiao Q, Wang J, Cai Z Q, Feng S D, Song Z Q, Huo B K, Li Z J and Wang L M 2023 *Chin. Phys. B* **32** 116401
[9] Mitka M, Góral A and Lityńska-Dobrzyńska L 2021 *J. Mater. Sci.* **56** 11071
[10] Lapér M L, Nunes E H, Houmard M and Wolf W 2023 *Mater. Res.* **26** e20230190
[11] Huttunen-Saarivirta E and Vuorinen J 2005 *Intermetallics* **13** 885
[12] Nguyen H V, Do N B, Nguyen THO, Nguyen C S, Trinh V T, Le HT and Jorge Junior A M 2023 *J. Mater. Res.* **38** 644
[13] Nascimento L 2021 *Orbital: Electron. J. Chem.* **13** 223
[14] Babilas R, Młynarek K, Łoński W, Łukowiec D, Kądziołka-GawełM, Czeppe T, Czeppe L and Temleitner L 2020 *Materials* **14** 54
[15] Li C, Dubovi J and Klein C 2022 *Mater. Charact.* **191** 112158
[16] Wolf W, Koga G Y, Schulz R, Savoie S, Kiminami C S, Bolfarini C and Botta W J 2020 *J. Therm. Spray Technol.* **29** 1195
[17] Abaei M, Rahimipour M R, Farvizi M and Eshraghi M J 2023 *International Journal of Engineering* **36** 1880
[18] Babilas R, Bajorek A, Spilka M, Radoń A and Łoński W 2020 *Prog. Nat. Sci.-Mater.* **30** 393
[19] Wang C, Li Z, Iefimov MO and Mordyuk B N 2023 *Surf. Eng.* **39** 532
[20] Huang J R, Takagiwa Y and Tsai A P 2020 *J. Phys. Conf. Ser.* **1458** 012011
[21] Shadangi Y, Bhatt S, Pradhan P, Tiwari A, Tripathi A, Chattopadhyay K and Mukhopadhyay N K 2023 *J. Alloys Compd.* **960** 170586
[22] Takagiwa Y, Maeda R, Ohhashi S and Tsai A P 2021 *Materials* **14** 5238
[23] Zheng J C 2022 *Research* **2022** 9867639
[24] Kamalnath M, Mohan B, Singh A and Thirumavalavan K 2020 *Mater. Res. Express* **7** 026535
[25] Kušter M, Samardžija Z, Komelj M, Huskić M, Bek M, Pierson G, Kouitat-Njiwa R, Dubois J M and Šturm S 2024 *Crystals* **14** 216
[26] Silveira A, e Silva LM, Oliveira T, Castro M, Figueiredo R, Bolfarini C, Botta W J and Wolf W 2022 *Mater. Lett.* **317** 132107
[27] Stagno V, Bindi L, Shibazaki Y, Tange Y, Higo Y, Mao H K, Steinhardt P J and Fei Y 2014 *Sci. Rep.* **4** 5869
[28] Stagno V, Bindi L, Park C, Tkachev S, Prakapenka V B, Mao H K, Hemley R J, Steinhardt P J and Fei Y 2015 *Am. Mineral.* **100** 2412
[29] Takagi S, Kyono A, Mitani S, Sugano N, Nakamoto Y and Hirao N 2015 *Mater. Lett.* **161** 13
[30] Hollister L S, Bindi L, Yao N, Poirier G R, Andronicos C L, MacPherson G J, Lin C, Distler V V, Eddy M P, Kostin A and Kryachko V 2014 *Nat. Commun.* **5** 4040
[31] Lin C, Hollister L S, MacPherson G J, Bindi L, Ma C, Andronicos C L and Steinhardt P J 2017 *Sci. Rep.* **7** 1637
[32] Paszkowicz W 2002 *Nucl. Instrum. Meth. B* **198** 142
[33] Soignard E, McMillan P F, Hejny C and Leinenweber K 2004 *J. Solid State Chem.* **177** 299
[34] Liu X L, Yu Z H, Li J F, Xu Z Z, Zhou C Y, Dong Z H, Zhang L L, Wang X, Yu N, Zou Z Q, Wang X L and Guo Y F 2023 *Chin. Phys. B* **32** 018102
[35] Ming X, He C P, Zhu X Y, Gou H Y and Wen H H 2023 *Chin. Phys. Lett.* **40** 017403
[36] Bragg W H and Bragg W L 1913 *Proc. R. Soc. Lond. Ser. A* **88** 428
[37] Tsai A P, Inoue A and Masumoto T 1989 *Mater. Trans. JIM* **30** 150
[38] Tsai A P, Inoue A, Masumoto T 1989 *Mater. Trans. JIM* **30** 666
[39] Tsai A P, Inoue A, Masumoto T 1988 *J. Mater. Sci. Lett.* **7** 322
[40] Fukamichi K, Masumoto T, Oguchi M, Inoue A, Goto T, Sakakibara T and Todo S 1986 *Journal of Physics F: Metal Physics* **16** 1059
[41] Inoue A, Kimura H and Masumoto T 1987 *J. Mater. Sci.* **22** 1758
[42] Sahnoune A, Ström-Olsen J and Zaluska A 1992 *Phys. Rev. B* **46** 10629
[43] Haberkern R, Lindqvist P and Fritsch G 1993 *J. Non-Cryst. Solids* **53** 303
[44] Klein T, Gozlan A, Berger C, Cyrot-Lackmann F, Calvayrac Y and Quivy A 1990 *Europhys. Lett.* **13** 129
[45] Shalaeva E, Chernyshev YV, Smirnova E and Smirnov S 2013 *Phys. Solid State* **55** 2205
[46] Xin X, Zhang S, Wan P, Liu L, Ding W, Li J, Wang Q and Dong C 2022 *Thin Solid Films* **753** 139272
[47] Chowdhury S, De Barra E and Laugier M. 2004 *Diamond Relat. Mater.* **13** 1625
[48] Oliver W C and Pharr G M 2004 *J. Mater. Res.* **19** 3
[49] Sakai M 1993 *Acta Metall. Mater.* **41** 1751
[50] Duan B, Zhang P, Wei X, Wang L, Wei D and Zhen D 2015 *Surf. Eng.* **31** 942
[51] Leyland A and Matthews A 2000 *Wear* **246** 1
[52] Chen L and Chen X 1992 *Phys. Status Solidi B* **169** 15
[53] Mihalkovič M and Widom M 2020 *Phys. Rev. Res.* **2** 013196
[54] Tcherdyntsev V, Kaloshkin S, Shelekhov E, Salimon A, Sartori S and Principi G 2005 *Intermetallics* **13** 841
[55] Asahi N, Maki T, Matsumoto S and Sawai T 1994 *Mater. Sci. Eng. A* **181** 841
[56] Dong Y, Lin X P, Xu R, Zheng R G, Fan Z B, Liu S J and Wang Z 2014 *J. Rare Earths Nov.* **32** 1048
[57] Avar B, Gogebakan M and Yilmaz F 2008 *Z. Kristallogr.* **223** 731